

Adaptive Power Allocation in Spaceborne-Assisted NOMA Systems for Integrated Terrestrial Communications

M Khalil, *Member, IEEE*, Ke Wang, *Senior Member, IEEE*, and Jinho Choi,
Fellow, IEEE

Abstract

This study introduces an innovative approach for adaptive power allocation in Non-Orthogonal Multiple Access (NOMA) systems, enhanced by the integration of spaceborne and terrestrial signals through a Reconfigurable Intelligent Surface (RIS). We develop an adaptive mechanism to adjust the power distribution between spaceborne and terrestrial signals according to variations in environmental conditions and elevation angles. This mechanism employs a sophisticated transition model that combines Gaussian Mixture Models with Log-Normal distributions to adaptively counteract the detrimental impacts of atmospheric attenuation and urban shadowing. These adaptive power adjustments significantly enhance system capacity, particularly improving the Signal-to-Interference-plus-Noise Ratio under diverse operational scenarios. Simulation studies confirm the efficacy of our method within an RIS-enhanced framework, showing an approximate 20% increase in system capacity through optimized power management between spaceborne and terrestrial signals.

Index Terms

non-orthogonal multiple access, reflecting intelligent surface, satellite-terrestrial integrated network, power allocation.

I. INTRODUCTION

Integrating satellite and terrestrial networks is crucial for advancing global connectivity and evolving sixth-generation (6G) communications. While terrestrial networks effectively cover

The authors are with the School of Engineering, RMIT University, Melbourne, Australia. Emails: muh.khalil@gmail.com, and ke.wang@rmit.edu.au. The author Jinho Choi with the Deakin University, Melbourne, Australia. Email: jinho.choi@deakin.edu.au

urban areas, they face challenges like limited coverage and have difficulty serving remote regions. Conversely, satellite networks broaden global coverage but struggle with challenges such as interference from shared frequency bands [1] and path loss [2]. Combining these networks improves service coverage and reliability, addresses key limitations, and extends access to underserved areas, ensuring more consistent communication services.

Reconfigurable Intelligent Surfaces (RIS) are revolutionizing 6G satellite-terrestrial networks, drawing keen interest from academia and industry. RIS technology enhances satellite signal pathways to terrestrial receivers, expanding channel range and improving signal quality. It optimizes transmissions to targeted users and reduces interference [3]. Recent studies, such as [4] on user scheduling and rate optimization, and [5] on specialized beamforming in RIS-enhanced networks, have mainly focused on beamforming and phase adjustments to enhance network performance and manage interference.

On the other hand, the increasing number of users has placed significant strain on spectrum resources, adversely affecting satellite-to-terrestrial communication rates [6]. To enhance spectral efficiency, non-orthogonal multiple access (NOMA) technology has been adopted, enabling the sharing of frequency channels. However, NOMA requires distinct channel conditions to effectively manage interference. Employing RIS technology, which adjusts signal phase shifts dynamically, can improve NOMA's performance by enhancing channel differentiation. Therefore, RIS-assisted NOMA enhances system spectral efficiency, capacity and user experience by managing interference more effectively [7]. In this context, the power allocation is essential, optimizing signal strength for each user based on their unique channel conditions to enhance NOMA efficiency. Recent studies like [8] and [9] have examined this aspect, yet they have limitations. Specifically, [8] does not incorporate RIS into the power allocation consideration and [9] neglects challenges in urban and varied geographic areas where satellite signals struggle with obstacles such as dense buildings, electronic interference, and multipath fading, all of which degrade communication link reliability and efficiency.

To address existing gaps, this study introduces a dynamic power allocation strategy for a NOMA-based RIS-assisted satellite-terrestrial integrated system. The proposed approach adjusts the power ratio between satellite and terrestrial signals in response to environmental conditions and elevation changes, optimizing signal transmission in urban and varied geographical areas. This significantly enhances network capacity and efficiency. By utilizing a transition model that combines Gaussian Mixture Models with Log-Normal distributions, we effectively mitigate

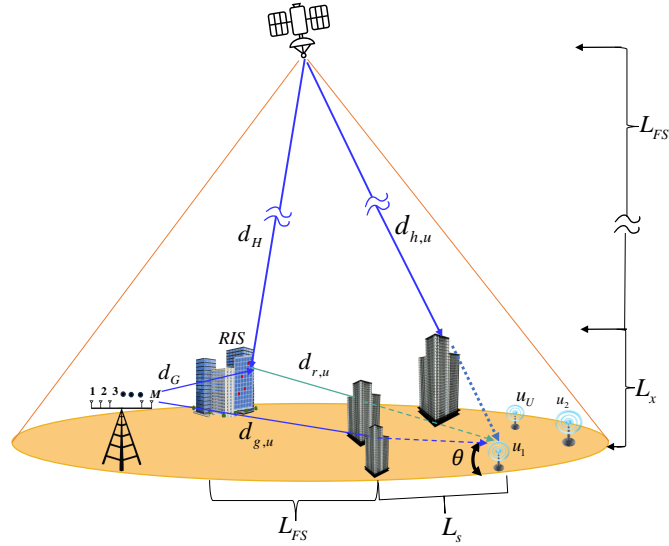


Figure 1. Architecture of an RIS assisted satellite-terrestrial integrated with NOMA

adverse effects such as atmospheric attenuation and urban shadowing. Simulation results indicate that the proposed dynamic power allocation method improves system capacity by approximately 20% highlighting its potential to enhance performance in RIS-assisted satellite-terrestrial communication systems.

II. SYSTEM MODEL

We consider a downlink communication setup within a network that integrates satellite and terrestrial signals through an RIS. This system encompasses a Base station (BS) equipped with M antennas, managing data links to U NOMA users, each with a single antenna. These users are grouped as $\mathcal{U} = \{1, 2, \dots, U\}$. The BS handles signal superposition and power allocation, and the users execute Successive Interference Cancellation (SIC) to decode signals, an essential process for ensuring clear communication, not provided by the satellite or RIS alone.

The RIS comprises N passive elements, each capable of modulating the phase of incoming signals. The reflection coefficient for the n^{th} element is denoted by $\varsigma_n = \Gamma_n e^{j\phi_n}$, where $\phi_n \in [0, 2\pi]$ represents the phase shift incurred by the n^{th} element, and Γ_n is the amplitude reflection coefficient, ideally assumed to be one. The capabilities of these elements are aggregated into the beamforming matrix $\Theta = \text{diag}([\varsigma_1, \varsigma_2, \dots, \varsigma_N])$, representing the direction of the reflected signals towards NOMA users.

The communication links in the system are characterized by specific channel vectors that characterize the propagation paths. The vector \mathbf{h}_u represents the channel from the satellite to the users, including the effects of atmospheric interactions on the satellite signal. The vector \mathbf{H} , where each entry corresponds to the transmission path from the satellite to one of the N elements of the RIS, is represented as $\mathbf{H} \in \mathbb{C}^{N \times 1}$.

For terrestrial communications, the vector $\mathbf{g}_{c,u} \in \mathbb{C}^M$ describes the direct path from the BS's M antennas to the u^{th} NOMA user, incorporating urban-induced multipath effects. The matrix $\mathbf{G} \in \mathbb{C}^{N \times M}$ maps the signal paths from the BS to the N elements of RIS. Additionally $\mathbf{f}_{r,u} \in \mathbb{C}^N$ indicates the channels from the RIS to the u^{th} NOMA users, illustrating how the RIS modifies and directs signals to enhance reception.

In our study, the Shadowed-Rician fading is considered for the satellite link incorporating both direct and scattered signal paths. On the other hand, the Rayleigh fading, is considered for the terrestrial links, which is typical for urban scattering environments.

In the system model, the BS employs a transmission strategy to efficiently target the u^{th} user by superposing individual user signals with varying power levels. The transmitted signal is represented as: $\mathbf{x}_c = \sum_{u=1}^U \mathbf{w}_u x_u$, where x_u is the data intended for the u^{th} user, normalized to ensure $\mathbb{E}\{|x_u|^2\} = 1$. The beamforming vectors $\mathbf{w}_u \in \mathbb{C}^{M \times 1}$ are designed to maximize transmission efficiency while satisfying the power constraint:

$$\sum_{i=1}^U \|\mathbf{w}_i\|^2 \leq P_t$$

where P_t represents the maximum allowable transmission power at the BS.

The received signal by the u^{th} user is given by:

$$y_u(u, \Theta, \theta) = \alpha(\theta) \left(\frac{\mathbf{h}_u^H}{\sqrt{PL_{s,u}}} + \frac{\mathbf{f}_{r,u}^H \Theta \mathbf{H}}{\sqrt{PL_{r,u}} \sqrt{PL_H}} \right) x_s + \sum_{k=1}^U \left(\frac{\mathbf{g}_u^H}{\sqrt{PL_{c,u}}} + \frac{\mathbf{f}_u^H \Theta \mathbf{G}}{\sqrt{PL_{r,u}} \sqrt{PL_G}} \right) \mathbf{w}_k x_k + n_u, \quad (1)$$

where $\alpha(\theta)$ is a control function that will be described in the following section, $PL_{r,u}$ represents the path loss between the RIS and u^{th} user, subject to frequency f and distance $d_{r,u}$, and it is given as

$$PL_{r,u} = L_{FS}(d_{r,u}, f) + L_s(\theta), \quad (2)$$

where $L_s(\theta)$ represents the shadowing loss as a function of the elevation angle. The path loss from the BS to u^{th} user, $PL_{c,u}$ is dependent on the frequency f and the distance $d_{c,u}$. It is

calculated as follows:

$$PL_{c,u} = L_{FS}(d_{c,u}, f) + L_s(\theta). \quad (3)$$

The path loss from the BS to the RIS, PL_G , is determined by the distance d_G , as $PL_G = L_{FS}(d_G, f)$. Finally, the path loss from the satellite to any user u^{th} ($PL_{s,u}$) is given by:

$$PL_{s,u} = L_{FS}(d_{r,u}, f) + L_\tau(f, \theta) + L_x(\theta) \quad (4)$$

where L_{FS} is the free-space path loss calculated as $20 \log_{10}(f) + 20 \log_{10}(d) - 147.55$, $L_\tau(f, \theta)$ represents atmospheric absorption loss, and $L_x(\theta)$ is an additional path loss defined by [2] that primarily stems from clutter loss due to buildings and other obstacles and includes shadow fading effects.

The expected power of the satellite-transmitted signal x_s is normalized as $E\{|x_s|^2\} = 1$, and the noise at the u^{th} user is modeled as an additive white Gaussian noise $n_{s,u} \sim \mathcal{CN}(0, \sigma_s^2)$, characterized by a zero-mean and a variance of $\sigma_{s,u}^2$. The noise variance is calculated as $\sigma_{s,u}^2 = \mathfrak{B}\mathcal{K}T$, where \mathfrak{B} is the receiver bandwidth, \mathcal{K} is, the Boltzmann constant, and T is environmental temperature. The Signal-to-Interference-plus-Noise Ratio (SINR) at user u is given by:

$$\text{SINR}(u, \Theta, \theta) = \frac{\left| \left(\frac{\mathbf{g}_u^H}{\sqrt{PL_{c,u}}} + \frac{\mathbf{f}_u^H \Theta \mathbf{G}}{\sqrt{PL_{r,u} PL_G}} \right) \right|^2}{\sum_{k>u}^U \left| \left(\frac{\mathbf{g}_k^H}{\sqrt{PL_{c,k}}} + \frac{\mathbf{f}_k^H \Theta \mathbf{G}}{\sqrt{PL_{r,k} PL_G}} \right) w_k \right|^2} \quad (5)$$

$$\frac{\alpha(\theta) \left| \left(\frac{h_u^H}{\sqrt{PL_{r,u}}} + \frac{\mathbf{f}_u^H \Theta \mathbf{H}}{\sqrt{PL_{r,u} PL_H}} \right) w_u \right|^2}{+ (1 - \alpha(\theta)) \left| \frac{h_u^H}{\sqrt{PL_{r,u}}} + \frac{\mathbf{f}_u^H \Theta \mathbf{H}}{\sqrt{PL_{r,u} PL_H}} \right|^2} + \sigma^2$$

where $\sum_{k>u}^U$ indicates the summation over all users with indices greater than u . We assume user indices are ordered by increasing power or decreasing channel quality, implying that user u can cancel the signals from all users with indices $k < u$, but not from those with indices $k > u$ during successive SIC.

The system capacity for user u is then calculated by:

$$C(u) = B \log_2 (1 + \text{SINR}(u, \Theta, \theta)), \quad (6)$$

where B is the system bandwidth.

III. DYNAMIC POWER ALLOCATION

We now focus on the NOMA-based downlink communication that integrates satellite and terrestrial signals. The performance of the satellite link varies significantly over the elevation

angle θ , and hence, here we focus on optimizing $\alpha(\theta)$ for the satellite communication link of NOMA users.

At lower elevation angles (θ_L), terrestrial signals, which are enhanced by the RIS, are normally dominating, while satellite signals are more susceptible to atmospheric attenuation and physical obstructions such as buildings or foliage. In such scenarios, the focus of RIS dynamic adjustment is on enhancing terrestrial signals to compensate for weak satellite signals. Conversely, at higher elevation angles (θ_H), where $\theta_H \rightarrow 90^\circ$, satellite signals typically exhibit increased strength and reliability due to the direct line-of-sight link. Hence, the RIS dynamic adjustment focuses on enhancing satellite signals.

The range $[\theta_L, \theta_H]$ delineates the transition over which the focus shifts from terrestrial signal to satellite signal. The sigmoid function is deemed particularly suitable for this transition due to its smooth and bounded nature, which realistically models the effectiveness of satellite signals relative to elevation angles. Mathematically, we define $\alpha(\theta)$ as:

$$\alpha(\theta) = \frac{1}{1 + e^{-r(\theta - \theta_0)}} \quad (7)$$

where r is a control parameter that adjusts the steepness of $\alpha(\theta)$'s transition, with θ_0 marking the midpoint where changes occur most rapidly. Here, r is critical to ensure the system adapts effectively to environmental influences.

For θ_L , the value of $\alpha(\theta)$ is given by $\alpha(\theta_L) = a = \frac{1}{1 + e^{-r(\theta_L - \theta_0)}}$, and similarly for θ_H as $\alpha(\theta_H) = b = \frac{1}{1 + e^{-r(\theta_H - \theta_0)}}$. Assuming θ_0 is the midpoint between θ_L and θ_H , expressed as $\theta_0 = \frac{\theta_L + \theta_H}{2}$, r is derived from the equations for a and b :

$$r = \frac{\log\left(\frac{1-a}{a}\right) - \log\left(\frac{1-b}{b}\right)}{\theta_H - \theta_L}. \quad (8)$$

Based on (8), r can be precisely tuned for the system's specific needs at both high elevation angles with prevalent excess path loss to low angles affected by shadowing. In this way, the satellite signal strength is adapted according to θ to compensate for environmental impacts. This approach incorporates stochastic factors like path loss and shadowing into $\alpha(\theta)$, enhancing its environmental responsiveness.

The signal attenuation due to shadowing for $\theta \leq \theta_0$ can be modeled as $e_L(\theta) \sim \mathcal{N}(\mu_L, \sigma_L^2)$, where μ_L and σ_L are the mean and standard deviation, respectively, of the logarithm of the environmental impact on signal attenuation due to shadowing [10]. For the signal attenuation due to excess path loss, a GMM can be employed to account for the combined effect of multiple sources of attenuation [11]. This model can be expressed as: $e_G(\theta) \sim \sum_{i=1}^K \pi_i \mathcal{N}(\mu_{H,i}, \sigma_{H,i}^2)$, where

K is the number of components, π_i are the mixture weights, and $\mu_{H,i}$ and $\sigma_{H,i}$ are the mean and standard deviation of each Gaussian component, respectively. This model considers different environmental factors contributing to signal attenuation for optimizing the communication system's performance under varying environmental conditions.

Now we focus on optimizing the transition between GMM and Log-Normal models at θ_0 . A controlled transition is facilitated using the hyperbolic tangent function:

$$e(\theta) = \mathcal{A} \tanh(\mathcal{B}(\theta - \theta_0)) \quad (9)$$

where \mathcal{A} and \mathcal{B} scale the amplitude and control the steepness of the transition in $e(\theta)$, respectively. \mathcal{A} is given as $\mathcal{A} = \psi |\mu_L(\theta_0) - \mu_H(\theta_0)| = \psi |\Delta\mu|$, where $\Delta\mu$ is the mean difference at θ_0 between the GMM and Log-Normal models, and ψ moderates the mean difference to prevent excessive amplitude, particularly in systems with substantial mean discrepancies.

Selecting ψ balances the model's sensitivity with the system dynamics, to meet operational demands and the acceptable impacts from environmental factors. ψ can be defined as $\psi = \frac{\mathcal{E}}{\Delta\mu + \lambda \sigma_c}$. The combined variance σ_c is calculated as $\sigma_c = \sqrt{\sigma_H^2(\theta_0) + \sigma_L^2(\theta_0)}$ to consider output variability. Additionally, λ is an adjustable parameter, initially set to 1, to fine-tune the influence of variance on the transition.

To balance the transition in $\alpha(\theta)$ without causing system instability or delays, we define the parameter \mathcal{B} as

$$\mathcal{B} = \frac{1}{C + \sqrt{\sigma_L^2(\theta_0) + \sigma_H^2(\theta_0)}}$$

where C is a constant ensuring \mathcal{B} does not become excessively large. This smooths transitions and avoids abrupt changes. The system adjusts $\alpha(\theta)$ dynamically using:

$$\alpha(\theta) = \frac{1}{1 + e^{-r(\theta - \theta_0) + \mathcal{A} \tanh(\mathcal{B}(\theta - \theta_0))}} \quad (10)$$

The value of r in (10) is determined by:

$$r = \frac{k' \Delta\mu}{\sigma_c (\theta_H - \theta_L)} \quad (11)$$

where k' is a scaling factor that adapts based on system feedback, defined initially as $k' = \frac{\Delta C_{\max}}{C_{\text{tar}}}$. Here, ΔC_{\max} estimates the maximum potential capacity change, and C_{tar} is the desired target capacity. For real-time updates, k' adapts according to: $k'_{\text{new}} = k'_{\text{old}} + \gamma(C_{\text{tar}} - C_{\text{obs}})$. C_{obs} is the currently observed capacity and γ is the learning rate calculated as $\gamma = \frac{\vartheta}{1 + \beta |e(t)|}$, where ϑ and β are scaling factors that set the initial responsiveness of γ and adjust the sensitivity based on the magnitude of the error $e(t)$, respectively. The range of β ensures that γ decreases significantly

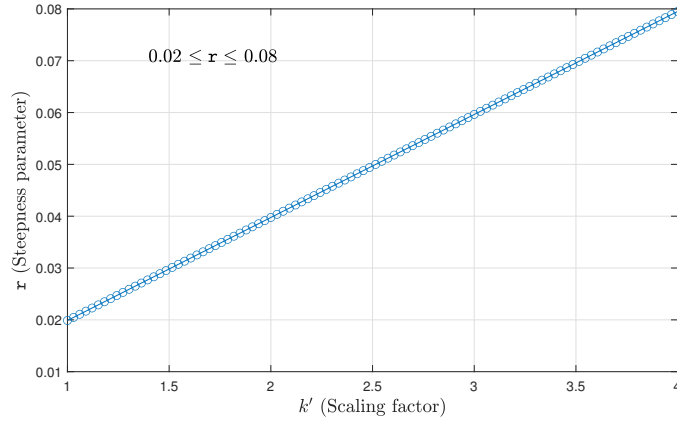


Figure 2. Range of r based on k' values under parameters: $\mu_L(\theta_0) = 0.5\mu_H(\theta_0) = 0.9$, $\sigma_H(\theta_0) = 0.1$ and $\sigma_L(\theta_0) = 0.2$

as the error increases, enhancing the stability.

The error $e(t)$ at time t calculated as $e(t) = C_{\text{tar}} - C_{\text{obs}}(t)$ drives the dynamic update of k' , enabling responsive system adjustments. A feedback loop updates k' continuously based on performance data: $k'(t+1) = k'(t) + \gamma e(t)$. This ensures the system adapts to changes and aligns with performance targets.

Given that r directly affects the behavior of $\alpha(\theta)$, which controls power distribution between satellite and terrestrial signal paths, it is crucial to establish a stable range for r to ensure smooth transitions in elevation angle θ without oscillations. We calculate the sensitivity of $\alpha(\theta)$ to changes in θ at the steepest point θ_0 as follows: $\left. \frac{d\alpha}{d\theta} \right|_{\theta=\theta_0} = \frac{r}{4}$. For stability, the peak derivative should not exceed γ , leading to the condition $r \leq 4\gamma$. Simulations indicate that system stability is compromised at $\gamma = 0.02$, setting an upper limit for r at 0.08. Conversely, the minimum responsive r value is found to be 0.02 when $\gamma = 0.005$. Using these values, we define k' range to maintain r within its range: $0.02 \leq k' \frac{k' \Delta\mu}{\sigma_c(\theta_H - \theta_L)} \leq 0.08$. Solving for k' : $0.02 \frac{\sigma_c(\theta_H - \theta_L)}{\Delta\mu} \leq k' \leq 0.08 \frac{\sigma_c(\theta_H - \theta_L)}{\Delta\mu}$. This approach ensures that the system remains stable and responsive across different conditions by carefully calibrating r and k' based on theoretical analysis and empirical observations. Fig. 2 shows the minimum and maximum values of r , visually representing the optimal range for r to maintain effective power allocation and stable system performance without excessive sensitivity to changes in elevation angle θ . By calculating the above parameters, the function $\alpha(\theta)$ is determined, which then guides the dynamic power allocations with $P_s(\theta) = \alpha(\theta) P_t$ and $P_b(\theta) = (1 - \alpha(\theta)) P_t$. To demonstrate the effectiveness of our dynamic power allocation strategy, we present several numerical examples using the following

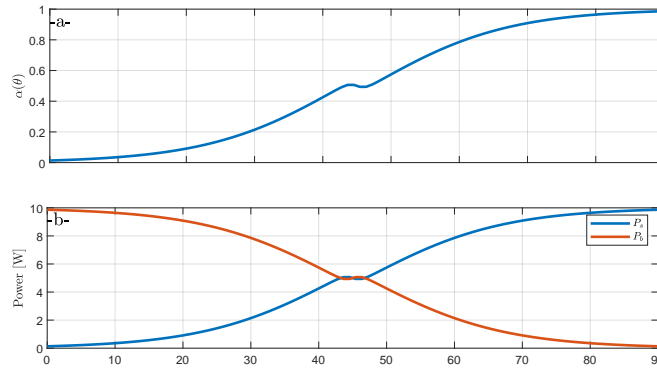


Figure 3. Effectiveness of dynamic power allocation strategy with elevation angles and $r = 0.08$

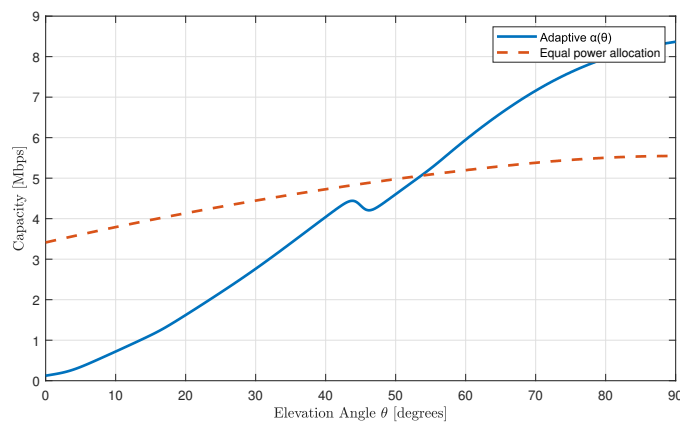


Figure 4. Capacity under dynamic and equals $\alpha(\theta)$ with elevation angle and $r = 0.08$

simulation parameters: $f = 2GHz$; $M = 6$; $N = 500$; $B = 1MHz$; and the number of users = 10.

Fig. 3-a shows the system's adaptive adjustments to the power allocation factor $\alpha(\theta)$ in response to changing elevation angles. The dynamic optimization of power distribution between satellite and terrestrial links is clearly illustrated, ensuring efficient resource use. In the middle elevation range, $\alpha(\theta)$ slightly decreases as the system transitions from prioritizing terrestrial to satellite signals, leading to a temporary reduction due to neither signal being clearly dominant. Fig. 3-b further illustrates the adjustments in power allocated for satellite P_s and terrestrial P_t across various elevation angles, particularly useful in environments with variable elevation angles.

Fig 4 illustrates the comparison of system capacity between two power allocation strategies: an optimal dynamic allocation using $\alpha(\theta)$ and an equal power allocation. The optimal strategy shows significant adaptability, enhancing system capacity at higher elevation angles with an

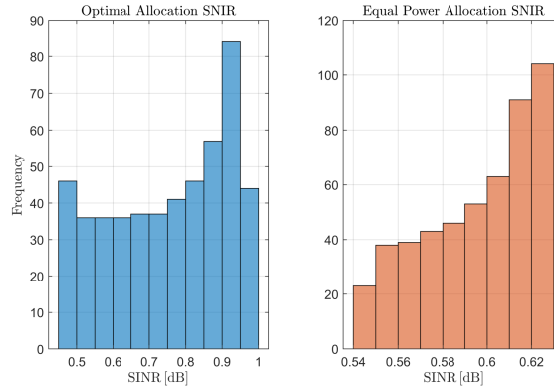


Figure 5. Effectiveness of dynamic power allocation in enhancing SINR at high elevation angles

improvement of approximately 20% over the static method. In contrast, equal power allocation performs well at lower angles but quickly plateaus, demonstrating limited flexibility. This underscores the advantage of adaptive power allocation in optimizing performance across varying conditions.

Fig. 5 shows histograms of SNIR distributions for high elevation angles, comparing optimal and equal power allocation strategies. Under equal power allocation, SNIR values are narrowly distributed around 0.5 to 0.6, indicating uniform but suboptimal performance. Conversely, dynamic power allocation significantly broadens the SNIR range, extending it from 0.4 to 0.9. This broader range highlights a significant enhancement in signal quality and adaptability, particularly at higher elevation angles where line-of-sight conditions are more favorable. The increase to higher SNIR values under optimal allocation reflects enhanced power utilization and corresponds to an approximate 27% improvement in SNIR, substantially boosting system performance and user experience in challenging conditions.

Fig 6 illustrates the impact of the steepness parameter r in the $\alpha(\theta)$ function on system capacity as the number of NOMA users increases. The parameter r controls how quickly power allocation between satellite and terrestrial signals adjusts with changes in elevation angle θ . With a lower r value (e.g., $r = 0.02$), the system maintains higher capacity for fewer users but experiences a sharp decline as the number of users increases, indicating less adaptability to high user loads. As r increases, the capacity decreases more gradually, particularly at higher elevation angles, showing improved responsiveness and better capacity maintenance in more challenging conditions. Overall, the figure shows that adjusting r effectively plays a crucial role in optimizing

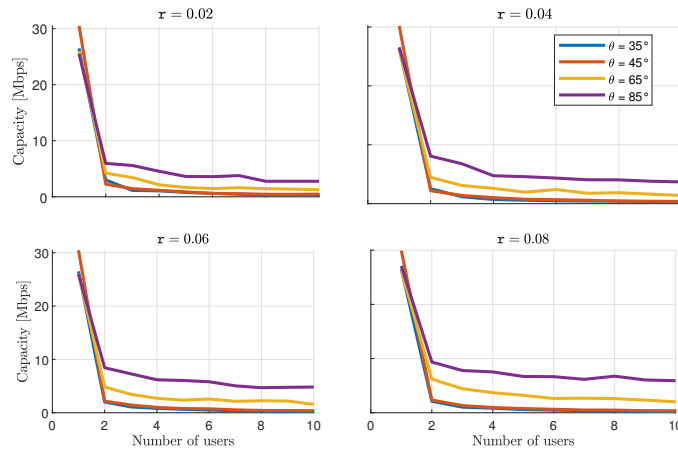


Figure 6. The impact of number user and θ on system capacity for different r

system performance across different numbers of users and elevation angles.

IV. CONCLUSION

This paper has introduced a dynamic power allocation method for NOMA-based RIS-assisted satellite-terrestrial integrated communication system. An adaptive function $\alpha(\theta)$ was proposed to dynamic adjust the power allocation between satellite and terrestrial links based on environmental conditions and elevation angle. By utilizing a transition model that combines GMM and Log-Normal distributions, the system smoothly adjusts power allocation, thereby enhancing capacity in the RIS-assisted satellite-terrestrial context. Simulation results validate the effectiveness of this approach, demonstrating enhanced communication capacity. This work highlighted the potential of adaptive signal management to enhance performance in communication systems facing diverse environmental challenges, setting a foundation for future advancements in the field.

REFERENCES

- [1] H. Dong, C. Hua, L. Liu, W. Xu, S. Guo, and R. Tafazolli, "Joint beamformer design and user scheduling for integrated terrestrial-satellite networks," *IEEE Transactions on Wireless Communications*, vol. 22, no. 10, pp. 6398–6414, 2023.
- [2] 3GPP, "3rd generation partnership project; technical specification group radio access network; study on new radio (nr) to support non-terrestrial networks (release 15)," 3rd Generation Partnership Project (3GPP), Tech. Rep. TR 38.811 V15.1.0, Jun. 2019. [Online]. Available: https://www.3gpp.org/ftp/Specs/archive/38_series/38.811/38811-f10.zip

- [3] Q. Wu and R. Zhang, "Intelligent reflecting surface enhanced wireless network via joint active and passive beamforming," *IEEE Transactions on Wireless Communications*, vol. 18, no. 11, pp. 5394–5409, 2019.
- [4] H. Dong, C. Hua, L. Liu, W. Xu, and R. Tafazolli, "Intelligent reflecting surface-aided integrated terrestrial-satellite networks," *IEEE Transactions on Wireless Communications*, vol. 22, no. 4, pp. 2507–2522, 2023.
- [5] S. Xu, J. Liu, Y. Cao, J. Li, and Y. Zhang, "Intelligent reflecting surface enabled secure cooperative transmission for satellite-terrestrial integrated networks," *IEEE Transactions on Vehicular Technology*, vol. 70, no. 2, pp. 2007–2011, 2021.
- [6] Y. Gu, T. Xu, K. Feng, Y. Ouyang, W. Du, X. Tian, and T. Lei, "ISAC towards 6G Satellite–Terrestrial Communications: Principles, Status, and Prospects," *Electronics*, vol. 13, no. 7, 2024.
- [7] R. Liu, K. Guo, X. Li, K. Dev, S. A. Khawaja, T. A. Tsiftsis, and H. Song, "RIS-empowered satellite-aerial-terrestrial networks with PD-NOMA," *IEEE Communications Surveys & Tutorials*, pp. 1–1, 2024.
- [8] K. Guo, H. Shuai, K. An, F. Zhou, T. A. Tsiftsis, X. Li, and M. Wu, "Power allocation and performance evaluation for noma-aided integrated satellite-hap-terrestrial networks under practical limitations," *IEEE Internet of Things Journal*, vol. 11, no. 7, pp. 13 002–13 017, 2024.
- [9] X. Liu, M. Lin, M. Tan, H. Guo, J. Ouyang, and T. Q. S. Quek, "Location-based downlink transmission scheme for irs-aided integrated satellite-terrestrial networks," *IEEE Transactions on Communications*, vol. 72, no. 2, pp. 1090–1104, 2024.
- [10] M. Khalil, J. Lin, and K. Wang, "Improving energy efficiency in satellite-to-ground communications with multiple reflecting intelligent surfaces," *IEEE Transactions on Green Communications and Networking*, pp. 1–1, 2024.
- [11] L. Bai, C.-X. Wang, G. Goussetis, S. Wu, Q. Zhu, W. Zhou, and E.-H. M. Aggoune, "Channel modeling for satellite communication channels at q-band in high latitude," *IEEE Access*, vol. 7, pp. 137 691–137 703, 2019.